Instability of the finite-difference split-step method applied to the generalized nonlinear Schrödinger equation. Part III: External potential and oscillating pulse solutions

T.I. Lakoba*

Department of Mathematics and Statistics, University of Vermont,
Burlington, VT 05401, USA

January 21, 2016

Abstract

This is the final part of a series of papers where we have studied numerical instability (NI) of localized solutions of the generalized nonlinear Schrödinger equation (gNLS). It extends our earlier studies of this topic in two ways. First, it examines differences in the development of the NI between the case of the purely cubic NLS and the case where the gNLS has an external bounded potential. Second, it investigates how the NI is affected by the oscillatory dynamics of the simulated pulse. The latter situation is common when the initial condition is not an exact stationary soliton. We have found that in this case, the NI may remain weak when the time step exceeds the threshold quite significantly. This means that the corresponding numerical solution, while formally numerically unstable, can remain sufficiently accurate over long times, because the numerical noise will stay small.

Keywords: operator splitting; numerical instability; nonlinear evolution equations.

*tlakoba@uvm.edu

1 Introduction

This work extends our study [1, 2] of numerical instability (NI) that may occur when the cubic nonlinear Schrödinger equation (NLS) is simulated by the finite-difference split-step method (fd-SSM). For the reader's convenience, we will briefly summarize the setup and main conclusions of [1], while also introducing modifications that will pertain to this work. Then we will explain our motivation for extending the results of [1].

We consider a generalized NLS of the form

$$iu_t - \beta u_{xx} + \big(\gamma|u|^2 + \Pi(x)\big)u = 0, \tag{1.1a}$$

where $\Pi(x)$ is a real-valued external potential, which in [1] was set to zero. Without loss of generality, we will assume

$$\beta < 0. \tag{1.1b}$$

The opposite choice, i.e. $\beta > 0$ (with the corresponding adjustment of signs of both γ and Π), will not affect either real or numerical instabilities of the solution, since Eq. (1.1a) is Hamiltonian. We assume that $\Pi(x)$ is bounded for all x, which explicitly *excludes*, e.g., $\Pi(x) \sim x^2$, as in the Gross–Pitaevskii equation. Our analysis will straightforwardly generalize if the term $(\gamma|u|^2 + \Pi(x))$ is replaced with a more general real-valued function $G(|u|^2, x)$, as long as G is smooth and bounded for all x and all finite $|u|^2$. That is the case, for example, for the saturable nonlinearity.

We simulate (1.1) with the fd-SSM:

(Nonlinear step):

$$\overline{u}(x) = u_n(x)\, \exp\left[i(\gamma|u_n(x)|^2 + \Pi(x))\Delta t\right] \tag{1.2a}$$

(Dispersive step):

$$i\frac{u^m_{n+1} - \bar{u}^m}{\Delta t} = \frac{\beta}{2}\left(\frac{u^{m+1}_{n+1} - 2u^m_{n+1} + u^{m-1}_{n+1}}{\Delta x^{\,2}} + \frac{\bar{u}^{m+1} - 2\bar{u}^m + \bar{u}^{m-1}}{\Delta x^{\,2}}\right). \tag{1.2b}$$

Here Δt and Δx are the time and space discretization steps, $u^m_n \equiv u(x_m, n\Delta t)$, and x_m is a point in the discretized spatial domain of length L: $-L/2 < x_m < L/2$. While this version of the SSM is not used as widely as the Fourier, or spectral, SSM (s-SSM), it is still a well-known method: see, e.g., Refs. [8]–[15] in [1] and Ref. [2] in [2]. For convenience of analysis, we assume periodic boundary conditions everywhere except in Section 6.3:

$$u(-L/2, t) = u(L/2, t), \qquad u_x(-L/2, t) = u_x(L/2, t). \tag{1.3}$$

This is consistent with the fact that the pulses whose dynamics we simulate are meant to have vanishing asymptotics at $|x| \to \infty$. In Section 6.3 we will show that absorbing, instead of periodic, boundary conditions can significantly affect the NI in certain situations.

In [1] we studied NI that can occur when the initial condition of (1.1) with $\Pi(x) \equiv 0$ is the exact soliton[1]

$$u(x, t) = U_{\rm sol}(x)\, \exp[i\omega_{\rm sol}t], \tag{1.4}$$

[1] More precisely, to facilitate repeatable development of NI, we added to that initial condition some white noise whose amplitude was several orders of magnitude below the soliton's amplitude. Yet, the noise's amplitude was large enough so that its high-wavenumber Fourier harmonics, from which NI could develop, were much larger than the machine round-off error. In what follows we will still be referring to initial conditions including such small white noise as being exact solitary waves.

with

$$U_{\rm sol}(x) = A\sqrt{2/\gamma}\,\mathrm{sech}\,(Ax/\sqrt{-\beta}); \qquad \omega_{\rm sol} = A^2. \tag{1.5}$$

We found that NI sets in when

$$\Delta t \gtrsim \Delta t_{\rm thresh} = \Delta x/(A\sqrt{-\beta}). \tag{1.6}$$

Let us make two side notes about this result. First, this NI threshold, $\Delta t_{\rm thresh} = O(\Delta x)$, is much more relaxed than the NI threshold for the s-SSM, which was found to be $O(\Delta x^2)$ both for the plane wave solution of (1.1) (with $\Pi(x) \equiv 0$) [3] and for the soliton [4]. Thus, the fd-SSM may be considerably more time-efficient (although having a greater spatial discretization error) than the s-SSM for simulation of solitary waves. Second, unlike for the s-SSM, for the fd-SSM the NI threshold is different for the plane wave and for the soliton: it was shown in [3] that for $\beta\gamma < 0$, the plane wave initial condition is numerically stable for any Δt.

The analysis of [1] explained the mechanism of the NI and a method[2] by which NI in similar situations can be analyzed. As for the NI threshold (1.6), its significance for practical simulations may appear to be limited because so is the significance of simulating a well-known exact solution of (1.1). Therefore, it is of interest to explore how the NI threshold may be modified when an external potential is included in (1.1) (or, more generally, when $(\gamma|u|^2+\Pi(x))$ is replaced by a more complicated expression). In such a case, a solitary wave of the form (1.4) may be first obtained numerically by solving the nonlinear eigenvalue problem

$$-\beta\,(U_{\rm sol})_{xx} + \big(\gamma|U_{\rm sol}|^2 + \Pi(x)\big)U_{\rm sol} = \omega_{\rm sol}U_{\rm sol} \tag{1.7}$$

by a relaxation method, and then its *physical* stability can be investigated by simulating (1.1) with the corresponding initial condition $U_{\rm sol}(x)$. Moreover, one may also want to numerically study the dynamics (e.g., long-term oscillations) of an initial condition that differs from the exact stationary solution $U_{\rm sol}(x)$ by a finite amount. In that case, can one expect that the NI threshold will be the same as found for the initial condition being the exact[3] $U_{\rm sol}(x)$?

The above two questions have motivated us to extend the analysis of [1]. In this work, we will first consider the situation where $\Pi(x)\not\equiv 0$ in (1.1) but the initial condition is very close (see above) to the exact solitary wave $U_{\rm sol}(x)$ of (1.7). We will find a counterpart of the NI threshold (1.6) and investigate how other properties of the NI change compared to the case of the purely cubic NLS. Then we will show that the threshold and other properties of the NI may be substantially modified when the initial condition differs from $U_{\rm sol}(x)$ by a finite (and even moderately small, on the order of 10%) amount. This latter statement may at first appear counter-intuitive. However, we emphasize, as we have done and demonstrated in Parts I and II of this study [1, 2], that properties of the NI depend not only on the numerical method and the underlying equation, but also on the simulated solution.

The fact that changing the initial condition by some 10% can change the NI threshold by 50% and more, raises the following issue: Why is it meaningful to even estimate that threshold if it may be so solution-dependent? Our answer, based on extensive simulations, is this. It is not only the NI threshold, but also the *growth rate* of the NI, which should be taken into account when choosing the

[2]The second side note above implies that this method is different from the principle of frozen coefficients based on the von Neumann analysis.

[3]see footnote before (1.4)

time step Δt for a simulation. If the NI is sufficiently weak, it may not significantly affect the numerical solution even over a long time. With this in mind, we will propose a (loosely defined) "practical NI threshold", which will turn out to be relatively robust to changing the initial condition. Moreover, we will demonstrate that such a "practical NI threshold" also approximately maintains the functional dependence of $\Delta t_{\rm thresh}$ on Δx. In fact, this dependence remains close to being $\Delta t_{\rm thresh} = O(\Delta x)$, as predicted for the exact soliton of the purely cubic NLS (see (1.6)).

In Section 2 we will state the evolution equation for a numerical error of Eq. (1.1) whose initial condition is the exact solitary wave $U_{\rm sol}(x)$ and derive from it the (approximate) NI threshold. In Sections 3–5 we will consider three choices of $\Pi(x)$ and γ in (1.4) that lead to scenarios of NI development that are different from the scenario described in [1]. In the cases considered in Sections 3 and 4, those differences will be qualitative and hence quite obvious, while in the case considered in Section 5, it will be less so. Nonetheless, it is this third scenario of the onset of NI that occurs when the pulse solution of (1.1) exhibits oscillatory dynamics due to the initial condition being different from the exact solitary wave by a finite amount. We will numerically study that situation in Section 6.

2 Equation for numerical error, and NI threshold

Properties of NI for the fd-SSM, including its approximate (see below) threshold, can be deduced from the equation satisfied by the numerical error with high wavenumbers k, which is where the NI is observed in the Fourier space [1]. Let the numerical solution $u(x, t_n)$ be represented as

$$u(x, t_n) = U_{\rm sol}(x)\, e^{i\omega_{\rm sol} t_n} + \tilde{u}(x, t_n), \tag{2.1}$$

where $\tilde{u}(x, t_n)$ is the numerical error and $U_{\rm sol}$ and $\omega_{\rm sol}$ are defined by (1.7). Below it will suffice for us to focus on the continuous-time limit, and thereby we will drop the discrete subscript 'n' of t_n. Then, repeating the steps of a similar derivation in [1], one finds that a quantity related to the high-k part of $\tilde{u}(x, t)$,

$$\psi(x, t) \equiv (-1)^n\, e^{-ik_{\max} x}\, e^{-i\omega_{\rm sol} t}\, \tilde{u}(x, t), \tag{2.2}$$

satisfies:

$$i\psi_t + \delta\psi - \psi_{\chi\chi}/(C|\beta|) + \gamma|U_{\rm sol}^2(\epsilon\chi)|\,(2\psi + \psi^*) + \Pi(\epsilon\chi)\,\psi = 0, \tag{2.3a}$$

where the asterisk denotes complex conjugation. Here we use the notations of [1]:

$$\epsilon = \Delta x/2, \qquad \chi = x/\epsilon; \tag{2.3b}$$

$$C = (\Delta t/\Delta x)^2, \qquad \delta = -\omega_{\rm sol} + 1/(C|\beta|). \tag{2.3c}$$

Note that in space, ψ can vary on a scale that is much smaller than $O(1)$ but greater than the grid spacing Δx [1]. Also, the faster — on the scale $O(\Delta x)$ — dependence of $\tilde{u}(x, t)$ on x is accounted for by the first factor on the r.h.s. of (2.2).

The evolution equation (2.3a) is reduced to an eigenvalue problem by a standard substitution $\big(\psi(\chi, t),\, \psi^*(\chi, t)\big) = \big(\phi_1(\chi),\, \phi_2(\chi)\big)\, e^{\lambda t}$:

$$\left(\frac{1}{C|\beta|}\partial_{\chi\chi} - \delta - \Pi(\epsilon\chi) - \gamma|U_{\rm sol}^2(\epsilon\chi)| \begin{pmatrix} 2 & 1 \\ 1 & 2 \end{pmatrix}\right) \vec{\phi} \,=\, i\lambda\sigma_3\vec{\phi}, \tag{2.4}$$

where $\vec{\phi} = (\phi_1, \phi_2)^T$ and $\sigma_3 = \mathrm{diag}(1, -1)$. By analogy with the external potential term $\Pi(x)$, we will refer to the $\gamma|U_{\rm sol}^2(x)|$ term as the "internal" potential of this eigenvalue problem. Solutions of (2.4) occur in quadruplets with eigenvalues $(\pm\lambda,\ \pm\lambda^*)$ [1]; hence the presence of NI corresponds to $\mathrm{Re}\lambda \neq 0$. From here a lower bound for the NI threshold can be deduced as follows. The matrix operators on both sides of (2.4) are Hermitian, and σ_3 on the right-hand side (r.h.s.) is not sign definite. The eigenvalues are guaranteed to be purely imaginary when the operator on the l.h.s. is sign definite [5]; otherwise they may be complex. The first term on the l.h.s. is negative definite, and hence the entire operator is guaranteed to be negative definite when

$$\delta + \min_x \Pi(x) + \min_{x,\,j}(\alpha_j\,\gamma|U_{\rm sol}^2(x)|\,) > 0, \tag{2.5}$$

where $\alpha_1 = 1$ and $\alpha_2 = 3$ are the eigenvalues of the matrix on the l.h.s. of (2.4). From the last inequality and (2.3c) one concludes that when

$$C \,<\, \frac{1}{|\beta|\,\big(\,\omega_{\rm sol} - \min_x(\Pi(x)) - \min_{x,\,j}(\alpha_j\,\gamma|U_{\rm sol}^2(x)|\,)\,\big)}, \tag{2.6}$$

the fd-SSM is guaranteed to be numerically stable. While one cannot generically show that it will be unstable whenever (2.6) is violated, in practice we have found (as earlier in [1] for $\Pi(x) \equiv 0$) that NI indeed sets in "soon" after C exceeds the threshold value given by the r.h.s. of that inequality. Therefore, (2.6) gives an approximate NI threshold, which from (2.3c) predicts that $\Delta t_{\rm thresh} = O(\Delta x)$. In the next three sections we will consider three distinct examples illustrating the above result.

3 External potential with multiple minima

In [1] we found that when $\Pi(x) \equiv 0$, numerically unstable modes are localized at the "tails" of the soliton, with their location depending on C. Here we will show that in the case where $\gamma > 0$ and $\Pi(x)$ has multiple local minima, unstable modes can be localized only near the locations of those minima. This will result in "stability windows", i.e. intervals of C values past the NI threshold where NI does not occur.

As an example, we considered Eq. (1.1) with

$$\beta = -1, \quad \gamma = 2, \quad \Pi(x) = 1.5\cos^2 x, \quad \omega_{\rm sol} = 1. \tag{3.1}$$

The numerical parameters were $L = 14\pi$ and $N = 2^{10}$ grid points. The corresponding soliton, found by the numerical method of [6], is shown in Fig. 1. In simulations, the initial condition was taken as that soliton plus noise with amplitude on the order of 10^{-10} (see the footnote before (1.4)). Inequality (2.6) yields the following approximate NI threshold:

$$C_{\rm thresh} \,\approx\, \frac{1}{|\beta|\,(\,\omega_{\rm sol} - \min_x(\Pi(x) + 1\cdot\gamma|U_{\rm sol}(x)|^2)\,)}. \tag{3.2}$$

Later on we will explain why this expression is bound to (slightly) underestimate the actual threshold value for C.

We have observed no NI until $C = 1.04$, at which point the unstable mode appeared as curve A in Fig. 1. Note that the mode is localized near a minimum of $\Pi(x)$. Given that the "internal" potential at this x is $2|U_{\rm sol}(x)|^2 \approx 0.01$, estimate (3.2) yields a smaller NI threshold: $C \approx 1.01$. The

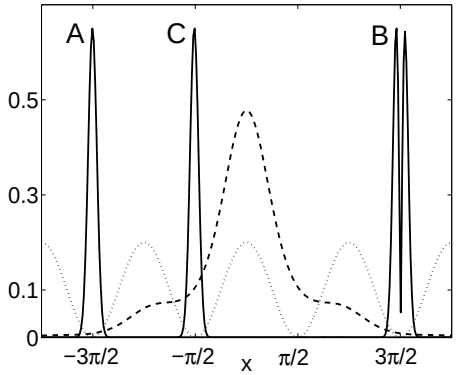

Figure 1: Dashed line: "Internal" potential $\gamma|U_{\rm sol}|^2$ ($\gamma = 2$), where $U_{\rm sol}$ is the solution of (1.1) and (3.1). The marked vertical scale pertains to this curve; all other curves are plotted with an arbitrary vertical scale. Dotted line: External potential $\Pi(x)$. Solid lines: Absolute value of unstable modes for various values of C. (Only one side of each mode is shown; in numerical simulations; one observes such a mode on both sides of the soliton; see Figs. 5(c) and 6 in [1].) A: $C \in [1.04, 1.05]$; B: $C \in [1.10, 1.11]$ (this is the second-order mode, similar to that in Fig. 7(a) in [1]); C: $C > 1.15$.

discrepancy (i.e., $C = 1.01$ versus $C = 1.04$) occurs due to neglecting the contribution of $\psi_{\chi\chi}$. Indeed, in the derivation of estimate (2.6) we set that contribution to zero, whereas it is strictly negative for a localized (or, more generally, spatially varying) mode. That negative contribution would decrease the denominator of (2.6) (and (3.2)) and hence increase $C_{\rm thresh}$. This effect is more conspicuous in the case of the soliton of (1.1), (3.1) than it was for the soliton of the purely cubic NLS considered in [1] because in the former case, the unstable mode is more localized (compare Fig. 1 and the thin solid curve in Fig. 5(b) in [1]), leading to a more negative contribution from $\partial_{\chi\chi}$. From the above discussion and Eq. (3.2), the contribution of operator $\partial_{\chi\chi}$ to the threshold value of C can be roughly estimated as:

$$\text{“}\partial_{\chi\chi}\text{”} \approx \frac{1}{1.04} - \frac{1}{1.01} \approx -0.03. \tag{3.3}$$

Let us clarify that the small absolute value of $\partial_{\chi\chi}$ agrees with the fact that while the mode is seen as narrow in x-space, it is still very wide in χ-space (recall (2.3b) and the note after (2.3)).

Continuing to increase C, we observed that in an interval $C \in [1.06, 1.09]$, NI disappears. This occurs due to the following. As C increases, the unstable mode "wants" to move towards the soliton's center, similarly to the situation with $\Pi(x) \equiv 0$; see Fig. 6(b) in [1].[4] As it moves away from $x = 3\pi/2$, the value of $\Pi(x)$ at the mode's location increases and this, according to (3.2), increases the NI threshold, leading to NI's disappearance.

As C continues to increase further, the second-order unstable mode moves from outside the soliton to the minimum of $\Pi(x)$ at $x = 3\pi/2$, and then NI reappears, being now caused by that second-order mode; see curve B in Fig. 1. With further increase of C, that mode moves towards the soliton's center and away from the minimum of $\Pi(x)$, and NI disappears again.

[4] One cannot *explain* this behavior without an analytical solution of the eigenvalue problem (2.4). Such a solution, however, is not possible at this time, as was explained for the simpler problem with $\Pi(x) \equiv 0$ in [1]. However, the tendency of the localized mode to shift towards the center of the soliton with the increase of C has been consistently verified by our numerical solution of (2.6).

It reappears when the first-order unstable mode moves into the minimum of $\Pi(x)$ closest to the soliton's center; see curve C in Fig. 1. In our numerical simulations this was observed starting at $C \approx 1.15$. On the other hand, estimate (3.2) yields $C \approx 1.11$, where we have used that at $x \approx \pi/2$ one has $2|U_{\rm sol}|^2 \approx 0.1$. However, if we add the contribution of $\partial_{\chi\chi}$ to the denominator of (3.2) and use (3.3), we obtain: $C \approx 1/(1 - 0.1 - 0.03) \approx 1.15$, which is in excellent agreement with the numerical result.

4 Bell-shaped potential; $\gamma < 0$

We will show that in this case, the unstable mode can appear either at the center or at the "tails" of the soliton. This should be contrasted with the previous case and with the case of $\Pi(x) \equiv 0$, where such a mode can appear *only* at the "tails".

As an example, we considered Eq. (1.1) with

$$\beta = -1, \quad \gamma = -1, \quad \Pi(x) = 6\mathrm{sech}^{\,2} x, \tag{4.1}$$

and used $L = 40$ and $N = 2^{10}$. Let us note that equations with $\gamma < 0$ are not too uncommon; for instance, the generalized NLS with saturable nonlinearity [7] provides an example of a realistic physical system with negative effective nonlinearity.

We will first describe how the soliton of (1.7), (4.1) depends on $\omega_{\rm sol}$, as this will explain different behaviors of NI observed in this case. By comparing the equation in question with the linear Schrödinger equation with a $\mathrm{sech}^{\,2} x$ potential, one can see that its soliton exists for $\omega_{\rm sol} \in (0,\, 4)$. At $\omega_{\rm sol} = 4 - 0$, it becomes vanishingly small and has the shape of $\mathrm{sech}^{\,2} x$. As $\omega_{\rm sol}$ decreases, the soliton becomes wider and its amplitude grows, so that at $\omega_{\rm sol} = 1$, one has $U_{\rm sol} = 2\mathrm{sech}\, x$. As $\omega_{\rm sol} = +0$, the soliton becomes very wide and its amplitude approaches $\sqrt{6}$. Amplitudes of the soliton at three values of $\omega_{\rm sol}$ are shown in Table 1.

The estimate of the the threshold beyond which NI *can* appear follows from (2.6):

$$C_{\rm thresh} \;\approx\; \frac{1}{|\beta|\,(\,\omega_{\rm sol} - \min_x(\Pi(x) - 3\cdot|\gamma||U_{\rm sol}(x)|^2)\,)}. \tag{4.2}$$

The validity of this estimate is supported by the first two lines of Table 1. We would like to stress three aspects of these results.

First, since for $\omega_{\rm sol} = 1$ and 2, $\min_x(\Pi - 3\cdot|\gamma||U_{\rm sol}|^2)$ occurs at $x = 0$, the unstable mode appears at the soliton's center rather than at its "tails". This mode looks like modes A and C in Fig. 1 except that it is located at $x = 0$.

Second, when the unstable mode occurs at the soliton's center, NI develops very rapidly with respect to parameter C. That is, lowering C by 0.001 compared to the value listed in the Table will suppress the NI entirely. At the listed value of $C_{\rm thresh}$, magnitude of unstable modes reaches $O(1)$ within $t \sim 100$. This is more than an order of magnitude faster than in the cases reported in Section 3 and [1] when C there exceeds $C_{\rm thresh}$ by 1%.

Third, the case $\omega_{\rm sol} = 3$ is different from that of $\omega_{\rm sol} = 1$ or 2 in that the unstable mode is predicted by (4.2) to be at the "tails" of the soliton. In that respect, it is similar to the mode discussed in [1] for the soliton of the purely cubic NLS. However, we have also observed substantial differences from the latter case. These new features of the NI are *not* specific to having $\gamma < 0$, and therefore we report them in a separate section, which follows next.

5 "Sluggish" NI

We begin by reporting our numerical results for the model (1.1), (4.1) with the initial condition corresponding to $\omega_{\rm sol} = 3$. For several values of C near the theoretical threshold $C_{\rm thresh} = 1/3$, we ran simulations up to $t = 50,000$. At $C = 0.345$, which is over 3% above the threshold, we have not observed any sign of NI. At $C = 0.350$, we have observed an order-of-magnitude growth (from 10^{-8} to 10^{-7}) of high-k harmonics in the Fourier spectrum. In comparison, for the same relative increase above the threshold, $(C - C_{\rm thresh})/C_{\rm thresh} \approx 5\%$, the NI *growth rate* of the pure NLS soliton was found in [1] to be about two orders of magnitude greater: see Fig. 3 there. As we continued to increase C, the NI has gradually become stronger; however, this was *not monotonic*. For example, the evolution of $|\mathcal{F}[u](k_{\rm max})|$ at two values of C is shown in Fig. 2(a), where a stronger NI corresponds to the smaller C. It is only past $C \approx 0.45$, i.e. 35% above the threshold predicted by (4.2), that the increase of NI's growth rate with C becomes monotonic.

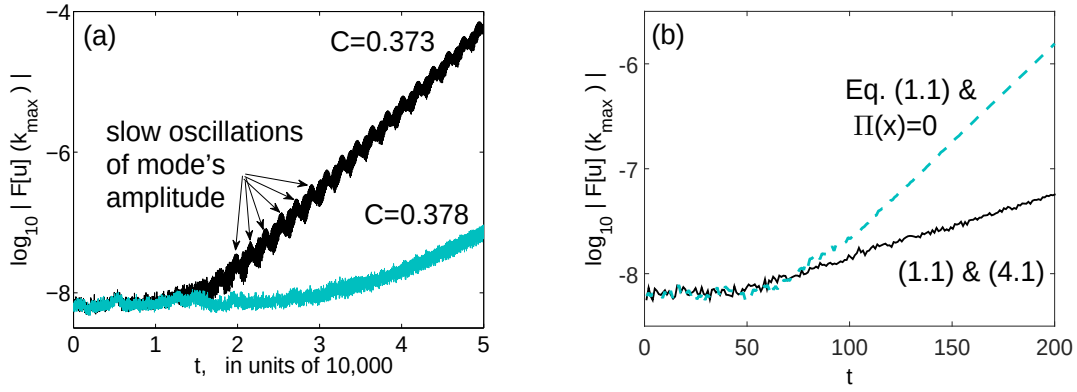

Figure 2: Evolution of the highest Fourier harmonic (see text). (a) For Eq. (1.1), (4.1) with $\omega_{\rm sol} = 3$. The lines appear thick because of oscillations on the scale of $t \sim 50$, which is not resolved in this figure. Note also slower oscillations with the period of $t \sim 2000$. (b) For the pure NLS ($\Pi(x) \equiv 0$ in (1.1)), $C = 1.1$ ($C_{\rm thresh} = 1$); for Eq. (1.1), (4.1), $C = 0.45$ ($C_{\rm thresh} = 1/3$).

We have called this NI "sluggish" due to its very slow, compared to the pure NLS case, development with the increase of C. Through extensive simulations, we have found that it occurs when the external potential $\Pi(x)$ is either wider or significantly taller (or both) than the "internal" potential $\gamma|U_{\rm sol}(x)|^2$. It is *not* specific to the particular sign of γ; for example, it also occurs when in (4.1) one takes $\gamma = +1$ and the initial condition with, e.g., $\omega_{\rm sol} = 5$, as well as for Eq. (5.6) below. We will now list features of this "sluggish" NI and then will provide some insight into them.

5.1 Features of "sluggish" NI

Let us emphasize that the characteristics of a "sluggish" unstable mode listed below are *generic*, i.e. were observed for several different potentials. More importantly, the same characteristics were also observed in many more cases, some of which are reported in Section 6, where the initial condition differed from the exact solitary wave $U_{\rm sol}(x)$ by a finite amount.

(i) The unstable mode could remain "hidden" for some time. This is most conspicuous when C is close to the threshold value predicted by (4.2) or, more generally, when the NI is weak. For

example, in the cases shown in Fig. 2(a), NI becomes visible only after $t \sim 15,000$ for $C = 0.373$ and $t \sim 25,000$ for $C = 0.378$. Motivated by this observation, we revisited our earlier simulations for the soliton of the pure NLS [1]. We have found the same "delayed" NI there as well, except that its starting time was considerably less; see Fig. 2(b).

(ii) The increase of NI with C is not monotonic; that is, as one increases C, NI may sometimes get substantially weaker than it was for a smaller value of C. This was illustrated by Fig. 2(a), and has also been observed in many other cases. (Note that for the two cases shown in Fig. 2(a), the small noise added to the initial condition $U_{\rm sol}(x)$ was the same.)

(iii) Growth of unstable modes *with time* is not monotonic, either. A mild example of it is also shown in Fig. 2(a); in some cases, we even observed oscillations of mode's amplitude of almost an order of magnitude.

(iv) Unstable modes in the case of a "sluggish" NI look different from typical unstable modes for the "non-sluggish" NI case of the pure NLS [1]. A comparison is shown in Fig. 3. In the x-space, both types of modes are almost zero within the soliton (and the external potential). However, while the mode in the "non-sluggish" case is localized (Fig. 3(b)), i.e. vanishes also *outside* the soliton, the mode in the "sluggish" case is not localized (Fig. 3(d)). In the k-space, the latter circumstance is reflected by a peak marked in Fig. 3(c), while the steep decay of the mode towards the soliton's center is reflected in a broad "plateau", similarly to what occurred for the unstable mode of the pure-NLS soliton (Fig. 3(a)). Eventually, as C becomes large enough, the shape of the unstable mode becomes qualitatively similar to that shown in Fig. 3(a,b).

Let us reiterate from the beginning of Sec. 5 that the *defining* feature of the "sluggish" NI is its slow, with respect to the increase of C, variation of the growth rate. In contrast, in the regime of "non-sluggish" NI, its growth rate increases sharply with C. Now, based on feature (iv), we can additionally delineate between "sluggish" and "non-sluggish" NIs based on whether the unstable mode is localized (has width of $O(1)$ or less) in the x-space. While this delineation is defined loosely, in practice is it quite sharp, as the transition between the two regimes occurs in a relatively narrow interval of C values.

(v) The fact that the unstable mode may be non-localized in x implies that the growth rate of "sluggish" NI can be affected by the length L of the computational domain, and this was indeed observed in our numerics.

(vi) Finally, as one decreases Δx, the relative range

$$\Delta C_{\rm rel,\,sluggish} \equiv (C - C_{\rm thresh,\,(4.2)})/C_{\rm thresh,\,(4.2)} \tag{5.1}$$

where the "sluggish" NI is observed (see next paragraph), decreases. For example, if in the simulations reported at the beginning of this subsection one takes $N = 2^{11}$ or $N = 2^{12}$ (i.e. decreases Δx two- and four-fold), then "sluggish" NI turns into "non-sluggish" one around $C = 0.42$ and 0.38, respectively. (Recall that $C_{\rm thresh,\,(4.2)} \approx 0.33$ in this case.) These values correspond to the $\Delta C_{\rm rel,\,sluggish} < 30\%$ and $\Delta C_{\rm rel,\,sluggish} \approx 15\%$, which should be contrasted with $C \approx 0.47$ for $N = 2^{10}$, where $\Delta C_{\rm rel,\,sluggish} > 40\%$.

5.2 Explanation of features of "sluggish" NI

Feature (i) — the "delayed" NI — has been previously reported and explained by us in [2]. Here we

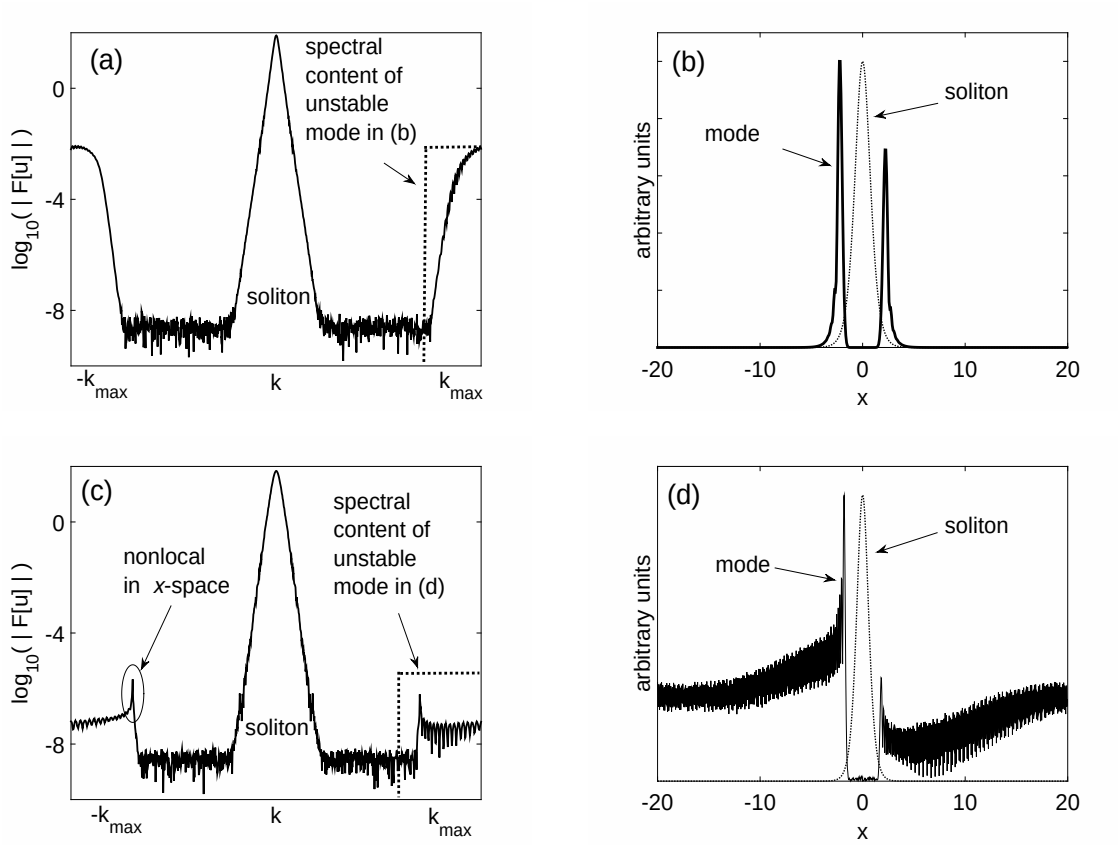

Figure 3: Fourier spectra of a numerical solution exhibiting "non-sluggish" (a) and "sluggish" (c) NI. Envelope in x-space of the unstable mode in the "non-sluggish" (b) and "sluggish" (d) cases. The spectral contents of these modes are contained in the boxes shown on the right of panels (a) and (c), respectively. The dotted lines in (b) and (d) show $|U_{\rm sol}(x)|^2$ for each case.

will repeat that explanation in rather general terms, so as to make it clear that the "delayed" NI is a generic scenario along which *any slow instability*, numerical or not, develops in an evolution equation with spatially varying coefficients.

Note that when monitoring the Fourier spectrum of the solution (on a logarithmic scale) to detect an instability, one follows the evolution of a specific harmonic with wavenumber, k_0. (Whether this k_0 is the edge of the spectral domain, $k_{\rm max}$, or the location of the harmonic with the largest amplitude (i.e., a "peak" as in Fig. 3(c)), is not important for the foregoing.) Since the governing equation for the evolution of the error is (2.3), then it is natural to expand that harmonic over the eigenfunction of (2.4):

$$\mathcal{F}[u](k_0,t) = \mathcal{F}[u](k_0,0)\left(c_{\rm most}\, e^{\lambda_{\rm most} t} + \sum_l c_l\, e^{\lambda_l t}\right). \tag{5.2a}$$

Here $\lambda_{\rm most}$ and λ_l are the eigenvalues of the most unstable mode and all other modes of (2.4), and

$c_{\rm most}$ and c_l are the corresponding expansion coefficients:

$$c_l = \left| \int_{-L/2}^{L/2} e^{ik_0 x} u^*_{\text{mode } l}\, dx \right| \Big/ \sqrt{L \int_{-L/2}^{L/2} |u_{\text{mode } l}|^2 dx}, \tag{5.2b}$$

and similarly for $c_{\rm most}$. A *point to note* is that $|c_{\rm most}|$ is less than 1 by some *finite* amount (see below). For example, for the NLS (1.1) with parameters (4.1) and with $\omega_{\rm sol} = 3$, or with parameters (5.6) considered below, one has

$$|c_{\rm most}| \sim 0.5. \tag{5.3}$$

(This statement appears plausible given that the most unstable mode, whose approximate shape is shown in Fig. 3(d), is quite far from a pure Fourier harmonic.) Over long time, the second term on the r.h.s. of (5.2a) becomes negligible compared to the first one; whence asymptotically:

$$\mathcal{F}[u](k_0, t) \approx \mathcal{F}[u](k_0, 0)\; c_{\rm most}\, e^{\lambda_{\rm most} t}. \tag{5.4}$$

Harmonic k_0 will become visible above the noise floor when $|\mathcal{F}[u](k_0, t)| > |\mathcal{F}[u](k_0, 0)|$. From (5.4) we obtain an estimate for the corresponding "delay" time:

$$t_{\rm delay} \sim \frac{\ln(1/|c_{\rm most}|)}{{\rm Re}\lambda_{\rm most}}. \tag{5.5}$$

Since $\ln(1/|c_{\rm most}|) = O(1)$ (see (5.3)), this time has the order of magnitude of $1/{\rm Re}\lambda_{\rm most} \gg 1$. In other words, the weaker the NI, the longer it takes the NI to become observable. In [2] we also explained why this time depends on the initial noise.

To provide insight into the remaining features listed in Section 5.1, we will report calculations for a different set of parameters of the NLS (1.1) than (4.1). By doing so we intend to demonstrate that a "sluggish" NI occurs not only when the the external potential is much taller than the "internal" one (as for (4.1) with $\omega_{\rm sol} = 3$), but also when it is wider. In fact, our simulations suggest that a "sluggish" NI will occur whenever $|\gamma U^2_{\rm sol}(x)| \ll |\Pi(x)|$ *at the "tails"* of the soliton. Thus, below we report results for the following parameters in (1.1):

$$\beta = -1, \quad \gamma = 2, \quad \Pi(x) = e^{-0.3x^2}, \quad \omega_{\rm sol} = 1. \tag{5.6}$$

The corresponding external and "internal" potentials are shown in Fig. 5 below. We also verified that respective results for parameters (4.1) with $\omega_{\rm sol} = 3$ are qualitatively the same. The eigenvalues and eigenfunctions of (2.4) with parameters (5.6) were computed numerically as explained in [1].

Feature (ii) is immediately explained by Fig. 4(a), which shows that the increase of max ${\rm Re}\,\lambda$ is not monotonic with C. (Without going into details about the spectrum's structure, explained in the caption, one can simply follow the circles in Fig. 4(a), which for almost all values of C correspond to the eigenvalue with the largest ${\rm Re}\,\lambda$.) This is most notably seen near $C = 1.035$, where the NI growth rate drops by almost an order of magnitude.

Feature (iii) is explained by noticing that below $C \approx 1.07$, there are multiple eigenvalues with very similar ${\rm Re}\,\lambda$. Their eigenmodes grow at very similar rates and interfere with one another, thus causing non-monotonic growth of the numerical error with time.

Feature (iv) is supported by Fig. 5(a). It shows the most unstable mode at $C = 1.051$, which is essentially nonlocalized and thus looks qualitatively similar to the mode shown in Fig. 3(d). This

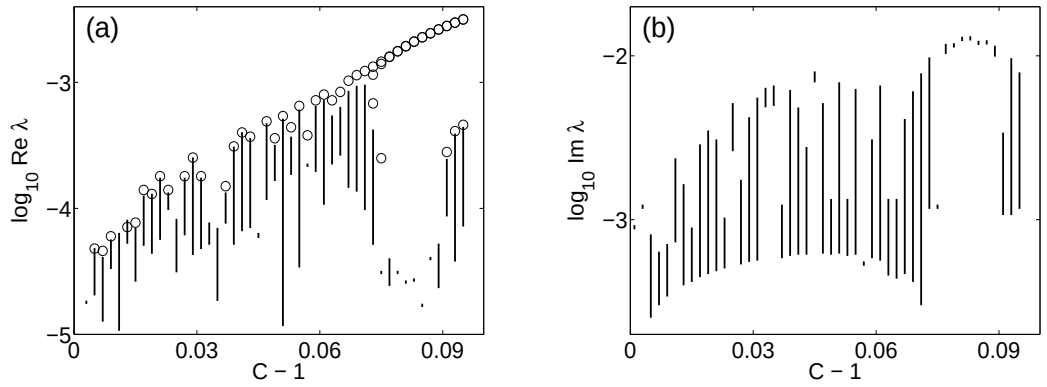

Figure 4: Eigenvalues of (2.4), (5.6) with $\mathrm{Re}\,\lambda > 0$. (Note that $C_{\mathrm{thresh},\,(4.2)} = 1$.) The spectrum corresponding to unstable eigenmodes has the following structure near the NI threshold. First, there is a purely real eigenvalue, $\lambda \equiv \Lambda_1$; for larger C values there may be two or more such real eigenvalues (Λ_2, Λ_3, etc.). Second, there is a group of complex eigenvalues $\lambda_j = \lambda_{\mathrm{r},\,j} + i\lambda_{\mathrm{i},\,j}$, $j = 1, \ldots J$. (The number of eigenvalues, J, in a group varies irregularly with C.) For some (typically, larger) C there may be a second and third group(s) of complex eigenvalues. Panels (a) and (b) show the eigenvalues of only the first such a group, as λ_{r}'s in the other group(s) are smaller. Within each group, as $\lambda_{\mathrm{r},\,j}$ decreases, $\lambda_{\mathrm{i},\,j}$ increases. In (a), circles show purely real eigenvalues, Λ_1 etc.. Vertical segments show the intervals of $\lambda_{\mathrm{r},\,j}$ (in (a)) and $\lambda_{\mathrm{i},\,j}$ (in (b)), $j = 1, \ldots J$, for the first group of complex eigenvalues. It can be seen that around $C = 1.077$, two purely real eigenvalues merge into a double eigenvalue, as has been observed earlier for the pure NLS case (see Appendix C in [1]).

should be compared to the localized mode at $C = 1.05$ for the pure NLS; see Fig. 5 in [1] or Fig. 3(b) here. Even at $C = 1.077$, where the two pairs of purely real eigenvalues have almost merged and far exceed real parts of other eigenvalues, the most unstable mode is still not quite localized (Fig. 5(b)).

Feature (v) is self-explanatory, as has been mentioned earlier. In our numerics we have observed that in its "sluggish" stage, where the most unstable mode is nonlocalized, NI gets, on average, weaker as L increases. However, this dependence is not monotonic. As C increases and the most unstable mode becomes essentially localized, the NI's growth rate, naturally, ceases to depend on L.

Feature (vi) is supported by Fig. 5(c), where we show that the most unstable mode becomes localized, and the NI ceases to be "sluggish", earlier (in terms of C values) for smaller Δx. A theoretical explanation of this feature would be based on an analytical solution of the eigenvalue problem (2.4), which clearly depends on $\epsilon \propto \Delta x$. However, as we have explained in [1] and noted in footnote 4, such a solution cannot be obtained with available tools.

In the next section we will encounter "sluggish" NI in a different context.

6 NI of oscillating solutions of Eq. (1.1)

In the the previous sections we have analyzed the NI on the background of solutions of the generalized NLS which have stationary shape. Here we will extend our study to the NI of solutions whose shape varies in time. As before, we will be concerned with the NI that is weak, i.e. takes a long time to develop. When the background solution's shape is changing, the development of weak NI is possible

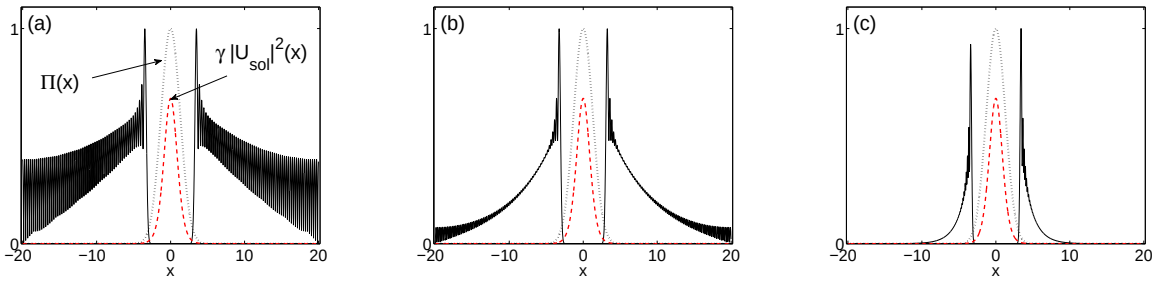

Figure 5: Envelopes of the most unstable mode (solid) and external (dotted) and "internal" (dashed) potentials. The equation is (1.1) with (5.6), and the domain length is $L = 40$. The vertical scale pertains to both potentials, while the amplitude of the mode is scaled to one. (a) $N = 2^{10}$, $C = 1.051$; (b) $N = 2^{10}$, $C = 1.077$; (c) $N = 2^{11}$, $C = 1.051$.

only when those changes are repetitive. Otherwise, factors leading to NI will not be able to accumulate coherently, and hence NI would not be able to occur (or will be weakened even further). Therefore, solutions where weak NI could occur must be periodic or near-periodic in time. We will show that NI on the background of such oscillating pulses is similar to the "sluggish" NI reported in Section 5.

Let us recall that one of the features of "sluggish" NI is that the unstable mode is not localized. Such a mode is, therefore, sensitive to the type of boundary conditions. In Sections 6.1 and 6.2 we will continue using periodic boundary conditions (1.3), the reason being that we want to compare the NI of oscillating pulses with that of exact solitons, considered in Section 5. In Section 6.3 we will consider absorbing boundary conditions and demonstrate that they eliminate "sluggishness" of the NI.

In all simulations reported below, we used $\beta = -1$ and $\gamma = 2$.

6.1 "Sluggish" NI of oscillating pulses

We began by simulating the purely cubic NLS ($\Pi(x) \equiv 0$ in (1.1)) with the initial condition and length of the computational domain given by:

$$u_0(x) = \mathrm{sech}\,(x) \cdot e^{-(x/3)^4} + 0.2\cos(2\pi x/L) + \xi(x), \qquad L = 20. \tag{6.1}$$

Here the exponential factor was used to ensure zero (to numerical accuracy), and hence periodic, boundary conditions at this shorter L than in the previous sections[5]. The role of the second term was to induce conspicuous oscillations; its specific, cosine, shape is not important and was chosen only to satisfy periodic boundary conditions. A white noise $\xi(x)$ in (6.1) had amplitude 10^{-10} and was included to facilitate controllable development of NI from its high-k Fourier components, as is explained in footnote 1 above.

At $t > 0$, the solution evolving from (6.1) resembles, near $x = 0$, a soliton whose amplitude and width oscillate in time. Away from the pulse's center, one observes a "pedestal", which oscillates as well. Due to periodic boundary conditions, oscillations of both the pulse and the "pedestal" are maintained indefinitely, although neither oscillation is exactly or even nearly periodic.

[5]This shorter L was chosen only for convenience, so that we could also use fewer grid points N and thereby run simulations faster.

We have found empirically that for C around 0.25, one observed a "sluggish" NI with all its features described in Section 5.1. In particular, we observed a "delayed" NI, whereby the instability may take a long time to develop. For example, for $N = 2^9$ and $C = 0.226$, it takes $t > 10,000$ for the NI to become barely visible above the noise floor; by $t = 50,000$ it grows only by half an order of magnitude. For $C = 0.265$, the most unstable Fourier harmonic rises just above the noise floor around $t \sim 6,000$ and grows by an order of magnitude by $t = 20,000$.

We have considered possible reasons that could cause "sluggish" NI in this case. From [1] and the examples in Sections 3–5 we know that numerically unstable modes can be found at the "tails" of the pulse. Then, could the "pedestal", which clearly affects the "tails" of the solution, have caused the "sluggish" NI? This hypothesis had appeared plausible, given our earlier observation (see Section 5.2) that "sluggish" NI appears when the external potential at the "tails" significantly exceeds the "internal" potential. (The "pedestal" could be thought as creating some effective external potential for the pulse.) However, we have answered this hypothesis to the negative by showing that "sluggish" NI is also observed for solutions that are either exactly or almost exactly periodic in time and do *not* have a "pedestal".

Such solutions were induced, for example, by the following initial conditions:

$$u_0(x) = 2\,\mathrm{sech}\,(x) + \xi(x), \qquad L = 40, \tag{6.2}$$

for the pure NLS ($\Pi(x) \equiv 0$), and

$$u_0(x) = \mathrm{sech}\,(x)\ (\,1 + 0.4(1 - 2x\tanh\,(x))\,) + \xi(x), \qquad L = 40, \tag{6.3}$$

for the generalized NLS (1.1) with $\Pi(x) = 1.5\exp(-0.2x^2)$. Initial condition (6.2) results in a well-known, time-periodic, analytical solution of the pure NLS (see Sec. 5.1 in [8]). The solution corresponding to (6.3) is a sech-like pulse whose amplitude oscillates between 1.08 and 1.44 almost periodically, with almost no dispersive radiation being emitted outside the pulse. Thus, neither of these solutions had a "pedestal", yet "sluggish" NI was observed for both of them (as well as for the solutions reported in the next subsection). From this we have concluded that it is, probably, the *oscillations* of the "tails" of the soliton that cause "sluggish" NI. This is the *main conclusion of this subsection.* Unfortunately, we were unable to explicitly relate the origin of the "sluggish" NI for oscillating pulses with that for stationary solitons in an external potential, as in Section 5.

6.2 Regarding threshold of "sluggish" NI

In the absence of a quantitative model for the "sluggish" NI of oscillating pulses, we have considered a question that may be posed by a researcher interested in avoiding NI in long-term simulations: For what relation between Δx and Δt does NI not grow above a certain amount (we used 'by one order of magnitude') at a certain simulation time (we used $t = 1000$)? In other words, what relation between Δx and Δt gives some "practical" NI threshold? We address this below. However, we remind the reader that, as we illustrated in Section 5 and in the first example in Section 6.1, "sluggish" NI may occur for a rather large range of C values. Therefore, it should be understood that this "practical" threshold is defined in subjective terms, which may depend on circumstances such as the required simulation time and the desired accuracy of the solution.

Our results in [1] and above (see (1.6), (3.2), and (4.2)) show that when the initial condition is *infinitesimally close* to an exact solitary wave, then the lower bound for the NI threshold satisfies the relation:

$$C_{\text{thresh, exact}} = \text{const} \quad \Leftrightarrow \quad \Delta t = O(\Delta x). \tag{6.4a}$$

This should be contrasted with a recent result of [9] (see Eq. (2.9) there), whose authors showed (by a method completely different from ours) that the lower bound for the NI must be

$$C_{\text{thresh, exact}} = O(\Delta x^{\,2}) \quad \Leftrightarrow \quad \Delta t \leq O(\Delta x^{\,2}). \tag{6.4b}$$

The analysis of [9], unlike ours, does *not* require the initial condition $u(x,0)$ to be infinitesimally close to the soliton[6]. Given the apparent discrepancy between the lower bounds (6.4a) and (6.4b), it is reasonable to ask: Which of the two bounds is the "practical" NI threshold closer to? Let us stress that a resolution of this question will have no implication to the issue of which of the two results is correct, because these results are analytical, while the "practical" NI threshold is empirical (and, as we have pointed out, can vary depending on requirements of a particular simulation). However, it will indicate which of the bounds (6.4a) and (6.4b) may be more "practical".

We have answered the above question by numerically simulating initial conditions (6.1)–(6.3) and several others, among which we report here the following two:

$$u_0(x) = 2.5\,\text{sech}\,(x) \cdot e^{-1.2(x/4)^4} + \xi(x), \qquad L = 15, \tag{6.5}$$

and

$$u_0(x) = \text{sech}\,(x)\ (\,1 + \varepsilon(1 - 2x\tanh(x))\,) + \xi(x), \qquad \varepsilon = 0.2, \quad L = 40. \tag{6.6}$$

Both of these were simulated for the pure NLS ($\Pi(x) \equiv 0$). Since the amplitude of the sech-like pulse in (6.5) is half-integer, that initial condition results in a dynamics that is most dissimilar to an $\mathcal{N}$-soliton solution (for an integer $\mathcal{N}$) [8]; the short length of the computational domain enhances that dissimilarity. Thus, such a solution represents a rather generic quasi-periodic (in time), pulse-like solution of the NLS. On the other hand, initial condition (6.6) was chosen because for $\varepsilon \ll 1$, it results in the soliton of amplitude $1 + \varepsilon^2$ plus a packet of dispersive radiation of order $O(\varepsilon)$, which oscillates near the soliton for a long time but eventually propagates away [10]. Note that the ε-term in (6.6) only minimally shifts the parameters of the original soliton [11]. The long-term quasi-periodic dynamics here is supported by the dispersive radiation repeatedly re-entering the computational domain due to periodic boundary conditions. We had to choose ε to be not too small since otherwise the "practical" threshold occurred almost exactly at the theoretical threshold $C = 1$ for the pure soliton, as found in [1].

For initial conditions (6.1)–(6.3), (6.5), (6.6) the dependence of the "practical" threshold, as defined above, on Δx is shown in Fig. 6. It is seen to be much closer to the dependence (6.4a), predicted in this work, than to (6.4b), predicted in [9]. The fact that it does not follow (6.4a) exactly agrees with feature (vi)[7] discussed in Section 5. Let us emphasize, again, that *all* features of the "sluggish" NI listed there were also observed for all the cases of the initial conditions considered in this section.

[6] However, it makes an assumption that $\tilde{u}(x) \equiv u(x,0) - U_{\text{sol}}(x)$ must be an even function: $\tilde{u}(-x) = \tilde{u}(x)$.

[7] It stated that the range of C values where "sluggish" NI is observed decreases with Δx.

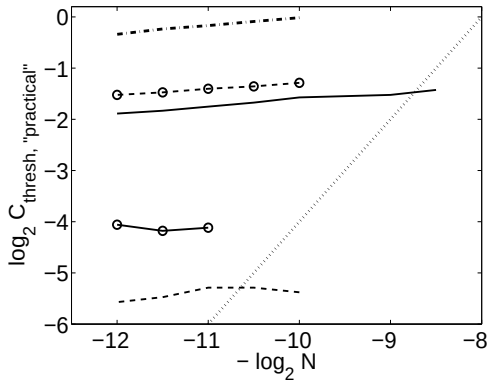

Figure 6: Dependence of the "practical" threshold on $N^{-1} \propto \Delta x$. Solid, dashed, and (thicker) dash-dotted lines pertain to the initial conditions (6.1), (6.5), (6.6), and solid and dashed lines with circles pertain to initial conditions (6.2), (6.3), respectively. Dotted line: the slope predicted by (6.4b). The smallest N in each case was dictated by ensuring a sufficiently small discretization error, whereas the largest, $N = 2^{12}$, was used to constrain the computational time.

6.3 Absorbing boundary conditions

As we have seen earlier (in Figs. 3(d) and 5(a)), the unstable modes in the "sluggish" stage of the NI are not localized. Therefore, they are expected to be modified if boundary conditions are not periodic. For solutions that are either exactly or almost periodic, like those generated by initial conditions (6.2) and (6.3), the natural boundary conditions are those which absorb the small amount of dispersive radiation (which may be caused, in particular, by the numerical discretization error) that leave the computational domain. The same type of boundary conditions are appropriate if one studies oscillations of a pulse near the center of a potential well or oscillations of two interacting pulses. Therefore, below we consider such absorbing boundary conditions. They can be implemented by multiplying the solution at each time step by a profile which equals unity in the bulk of the computational domain but gradually decreases towards the edges. This decrease does not have to occur all the way to zero, because repeated multiplication by such a profile will cause the solution to still vanish at the edges. We will report results for the absorbing profile

$$\mathrm{absbc}(x) \;=\; \begin{cases} 1, & |x| \le 0.35L \\ \exp\left[-0.04\left(\frac{|x|/L-0.35}{0.15}\right)^2\right], & |x| \in (0.35L,\, 0.5L]; \end{cases} \tag{6.7}$$

similar results were obtained when its parameters had been varied so as to still satisfy the general description given above. The resulting solution of (1.1) with the absorbing boundaries (6.7) gradually approaches zero for $|x| \in (0.35L,\, 0.5L]$.

Among the initial conditions listed above we chose (6.2), leading to the exactly time-periodic and localized solution of the pure NLS. (Note that absorbing boundary conditions would have qualitatively changed dynamics of solutions induced by initial conditions (6.1), (6.5), and (6.6), because their quasi-periodic motion is supported by repeated re-entrance of dispersive radiation through the periodic

boundaries.) We used $L = 60$ and $N = 3 \cdot 2^{11}$; this larger (than in Section 6.1) computational domain allowed us to neglect the effect of the absorbing boundaries on the solution.

As a benchmark, we simulated this case without the absorber. The growth rate of the most unstable mode observed in the range $C \in [0.065, 0.080]$ is plotted in Fig. 7(a) with the dashed line. The growth rate corresponds to $\mathrm{Re}(\lambda)$, with λ being defined before (2.4), and is estimated as

$$\mathrm{Re}\,(\lambda)|_{\mathrm{est}} = \frac{\ln\left(\max_k |\mathcal{F}[u](k,t_2)|\right) - \ln\left(\max_k |\mathcal{F}[u](k,t_1)|\right)}{t_2 - t_1}. \tag{6.8}$$

Here $\max_k$ is taken over wavenumbers lying outside the solution's spectrum that lies above the noise floor, and times $t_{1,2}$ are taken on the approximately linear part of the evolution of the logarithm of the unstable mode's amplitude (as illustrated in Fig. 2). The slow and non-monotonic variation of this rate with $C < 0.078$ suggests that the NI is "sluggish" there, while it ceases to be "sluggigh" around $C = 0.078$. In the same figure we also plot (with the solid line) the growth rate of the NI that occurs in the presence of absorber (6.7). As one can see, the absorbing boundary conditions eliminate the "sluggishness" of the NI. On the other hand, for $C > 0.078$, where the unstable mode becomes increasingly localized, the type of boundary conditions no longer affects the NI growth rate. In Fig. 7(b) we show the unstable mode obtained with the absorber very near the NI threshold. It looks similar to the nonlocalized mode shown in Fig. 3(d), except that it gradually decays in the near-edge region where $\mathrm{absbc}(x) < 1$.

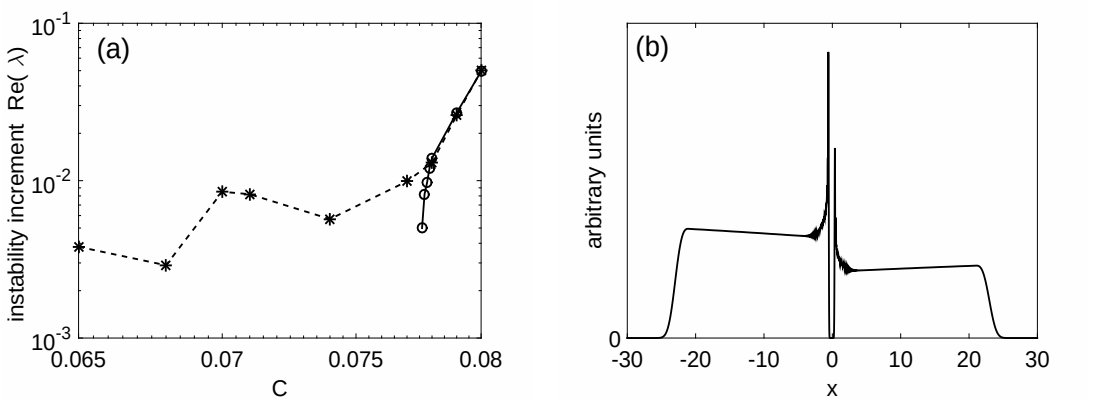

Figure 7: (a) Estimated growth rates of the NI with (solid line) and without (dashed line) the absorber. The symbols represent the actual data points, while the lines are guide for the eye. Note that there is no NI in the case with the absorber for $C \leq 0.0775$, which we verified by extending our simulations to $t = 25,000$. (b) The envelope of the unstable mode in the case with the absorber for $C = 0.0777$.

7 Summary of results

We have extended our earlier study [1] of NI of a soliton of the NLS in two directions.

First, we considered changes that inclusion of an external potential and switching the sign of nonlinearity can cause to properties of the NI, while the *initial condition is taken infinitesimally close to the stationary soliton* (as in [1]). In Section 3 we found that for a potential with multiple

local minima outside the soliton's center, there may exist "stability windows" past the NI threshold. That is, for $\Delta t \in (a, b)$ with $a > \Delta t_{\text{thresh}}$, the soliton can be numerically stable. This occurs due to an interplay of two effects. On one hand, for Δt exceeding the NI threshold by a sufficiently small amount, numerically unstable modes can exist only near the minima of the potential. On the other hand, the location of the modes, x_{unst}, depends on the parameter $C = (\Delta t/\Delta x)^2$. Thus, it is only when $x_{\text{unst}}(C)$ nearly coincide with the potential's minima that NI can occur.

When (effective) nonlinearity of the generalized NLS is defocusing, as in the example in Section 4, unstable modes can (but not always do) exist at the center of the soliton rather than at its "tails", as in [1]. In that case, the NI growth rate is much greater than when the unstable modes occur at the "tails". Equivalently, the numerical solution obtained for $\Delta t > \Delta t_{\text{thresh}}$ becomes invalid after a much shorter time when numerically unstable modes are localized at the soliton's center than at its "tails".

When the external potential at its "tails" is much greater than the internal one there, as in Section 5, we have observed "sluggish" NI. Its hallmark is that this NI remains weak for a range of C values exceeding the NI threshold by several tens percent; hence the name. The corresponding unstable modes differ from those of a "non-sluggish" NI, considered in [1] and Sections 3 and 4, in that they are delocalized, i.e. occupy the entire computational domain (except for the soliton's center). Eventually, i.e. for sufficiently large C, those modes become localized at the soliton's "tails", which is accompanied by a considerable increase in the NI growth rate.

Let us also mention that in all of the above scenarios with an external potential, the soliton promptly disintegrates once the numerical noise reaches magnitude of order one. This should be contrasted with the behavior of a numerically unstable soliton in the NLS without an external potential [1], where the soliton would drift for a long time before eventually disintegrating due to accumulation of dispersive radiation.

The second direction in which we have extended the study in [1] was the consideration of an *NI of an oscillating solution*. Such solutions often occur when the initial condition differs from the exact stationary soliton by a finite amount; examples are given in Section 6. We were unable to make any analytical progress in this case, but have empirically found that NI there is also "sluggish". In practical terms, this means that one can simulate the solution with a time step exceeding the NI threshold by several tens percent and still not notice a decrease in accuracy, as the numerical noise can remain sufficiently small. This motivated us to consider a "practical" NI threshold, defined as a Δt for which the magnitude of the most unstable mode does not grow by more than a given factor over a given time. We have shown that this "practical" threshold approximately follows the dependence $\Delta t_{\text{thresh, practical}} = O(\Delta x)$, which we have earlier derived [1] as the lower bound of the exact NI threshold for the soliton initial condition of the NLS. Finally, we have demonstrated that imposition of absorbing, instead of periodic, boundary conditions eliminates "sluggishness" of the NI.

Acknowledgement

This research was supported in part by NSF grant DMS-1217006.

References

[1] T.I. Lakoba, Instability of the finite-difference split-step method applied to the nonlinear Schrödinger equation. Part I: Standing soliton, submitted.

[2] T.I. Lakoba, Instability of the finite-difference split-step method applied to the nonlinear Schrödinger equation. Part II: Moving soliton, submitted.

[3] J.A.C. Weideman and B.M. Herbst, Split-step methods for the solution of the nonlinear Schrödinger equation, SIAM J. Numer. Anal. 23 (1986), 485–507.

[4] T.I. Lakoba, Instability analysis of the split-step Fourier method on the background of a soliton of the nonlinear Schrödinger equation, Num. Meth. Part. Diff. Eqs. 28 (2012), 641–669.

[5] I.M. Gelfand, *Lectures on linear algebra* (Interscience Publishers, New York, 1961), Sec. 15.

[6] T.I. Lakoba, J. Yang, A generalized Petviashvili iteration method for scalar and vector Hamiltonian equations with arbitrary form of nonlinearity, J. Comp. Phys. 226 (2007), 1668–1692.

[7] M. Segev, G.C. Valley, B. Crosignani, P. DiPorto, A. Yariv, Steady-state spatial screening solitons in photorefractive materials with external applied field, Phys. Rev. Lett. 73 (1994), 3211–3214.

[8] J. Satsuma, N. Yajima, Initial value problems of one-dimensional self-modulation of nonlinear waves in dispersive media, Suppl. Progr. Theor. Phys. 55 (1974), 284–306.

[9] D. Bambusi, E. Faou, and B. Grébert, Existence and stability of solitons for fully discrete approximations of the nonlinear Schrödinger equation, Numer. Math. **123**, 461–492 (2013).

[10] E.A. Kuznetsov, A.V. Mikhailov, I.A. Shimokhin, Nonlinear interaction of solitons and radiation, Physica D 87 (1995), 201–215.

[11] D.J. Kaup, T.I. Lakoba, Variational method: How it can generate false instabilities, J. Math. Phys. 37 (1996), 3442–3462.

ω_{sol}	$\max \lvert U_{\text{sol}} \rvert$	$\min \left(\Pi - 3\gamma \lvert U_{\text{sol}} \rvert^2\right)$	mode's location	$C_{\text{thresh, (4.2)}}$	$C_{\text{thresh, numer}}$
1	2	-6	center	0.144	0.145
2	1.657	-2.237	center	0.237	0.241
3	1.187	0	"tail"	0.334	see Sec. 5

Table 1: NI of the soliton of Eq. (1.7), (4.1); see text for details. The last two columns list theoretical and numerically observed values for the NI threshold.